Journal of Hydroscience and Hydraulic Engineering
Vol. 16, No. 1, May, 1998, 9-25

A study on a wind field when a cold air flow that causes snowfall around Sapporo

By

Keisuke Nakayama

Research Associate, Department of Civil Engineering,
Hokkaido University, Sapporo, Japan

Kazuyoshi Hasegawa

Research Associate, Department of Civil Engineering,
Hokkaido University, Sapporo, Japan

and

Mutsuhiro Fujita

Professor, Department of Civil Engineering,
Hokkaido University, Sapporo, Japan

SYNOPSIS

Snow falls around Sapporo when a cold air flow occurs over Ishikari Bay. Therefore predicting a wind field is important for predicting snowfall. First, the horizontal convection caused by a temperature difference of about 20 ℃ between the sea and a cold air flow was numerically analyzed. Second, the wind field was analyzed, then the release rate of latent heat between the convection area and the compensation area was estimated using a convection model.

It was found that the effect of the actual horizontal convection is weak and that the vertical profile of vertical velocity in the convection model was similar to the observed profile. The results also showed that the possibility of the change from convection to low pressure over the Ishikari Bay area is confirmed using the release rate of latent heat.

INTRODUCTION

There are many days of snowfall during the winter around Sapporo, and the heavy snowfalls cause many social problems in the city such as long traffic jams. Sapporo is located on a plain area, which has snowfalls in winter along the coastal area of the Japan sea. There are many types of snowfall in this area, and the most characteristic one causes snow clouds accompanying a cold air flow.

During the night, air that is colder than the upper air (monsoon) occurs over the land around Ishikari Bay due to the difference in thermal capacity between the land and sea. This cold air, which is known as "a cold air flow", runs off the mountain slope in an east-west direction. The cold air flow extends over the Ishikari Bay. It covers over the center of Ishikari Bay against monsoon. The cold air flow behaves like a cold front and snow clouds occur. Snow clouds moved over Sapporo in a commonly appeared northwesterly wind. Then they bring snowfall (5).

In our previous studies, using gravity current theory we were able to predict the distance of the extended cold air flow from the coastal line, which is an important factor in determining the location of the snow clouds (7)(8). Clarification of the occurrence and movement of snow clouds is important in order to predict snowfalls in Sapporo.

There have been many previous studies on methods to predict the movement of clouds. These methods of prediction include the use of the pseudo-moist adiabatic

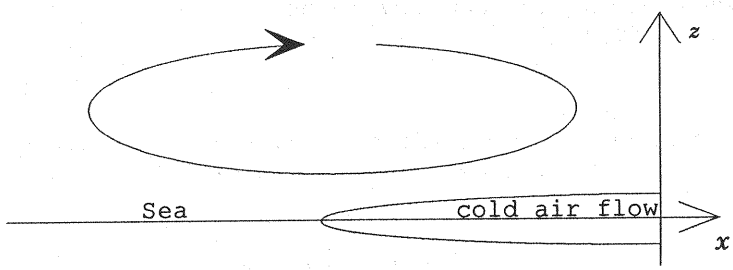

Fig. 1 Model of the horizontal convection

process (6) and the use of the convection term (10). However, these studies have only considered the prediction of cloud movement after the snow clouds have formed and do not consider the formation mechanism of snow clouds. Moreover, they did not investigate the distinctive structure that snow clouds occur at the edge of the front.

Many studies have also been carried out to determine the characteristics of an extended cold air flow. These studies point out the significance of the following factors: the shape of the cold air flow, the change from a cold front to a warm front by the growth and decline of the cold air flow, and the K-H instability between the cold air flow and monsoon. (4)(13)(14)(15). On the other hand, other studies have pointed out the significance of the shape of the gravity current, which is assumed to be like as see breeze (2)(3)(11)(12). Although these studies have provided a lot of useful data for the analysis of snow clouds, there have been no attempts to apply these data to snowfall prediction.

The aims of the present study are to analyze the wind field with consideration to the difference in air temperature over land and sea, to develop a model of vertical convection using cumulus convection theory, and to investigate the possibility of the development of cumulus convection to low pressure over Ishikari Bay area.

HORIZONTAL CONVECTION

When the cold air flow occurs, around the Ishikari Bay area, the temperature difference between the cold air flow and air over the sea in winter is as much as 20 ℃. In this section we analyze steady and unsteady wind fields with special regard to the temperature distribution.

Steady wind field

Fig. 1 shows the horizontal convection model developed in the present study. The height of the extended cold air flow is much less than the height of the model area. In this analysis the shape of the cold air flow is regarded as an ellipse. Eq. 1 is the basic equation and Eq. 3 shows the dimensionless equations obtained from Eq. 2, where ψ = dimensionless stream function; ω = vortisity; T = temperature; α = cubical expansion coefficient of air; ν = viscosity coefficient; κ = thermal diffusivity; Γ =

$$\begin{cases} \dfrac{\partial \psi_*}{\partial z_*}\dfrac{\partial \omega_*}{\partial x_*} - \dfrac{\partial \psi_*}{\partial x_*}\dfrac{\partial \omega_*}{\partial z_*} + \alpha g \dfrac{\partial T_*}{\partial x_*} = \nu\left(\dfrac{\partial^2 \omega_*}{\partial {x_*}^2} + \dfrac{\partial^2 \omega_*}{\partial {z_*}^2}\right) \\ \omega_* = \dfrac{\partial^2 \psi_*}{\partial {x_*}^2} + \dfrac{\partial^2 \psi_*}{\partial {z_*}^2} \\ \dfrac{\partial \psi_*}{\partial z_*}\dfrac{\partial T_*}{\partial x_*} - \dfrac{\partial \psi_*}{\partial x_*}\dfrac{\partial T_*}{\partial z_*} - \Gamma \dfrac{\partial \psi_*}{\partial x_*} = \kappa\left(\dfrac{\partial^2 T_*}{\partial {x_*}^2} + \dfrac{\partial^2 T_*}{\partial {z_*}^2}\right) \end{cases} \tag{1}$$

$$\begin{cases} z = \dfrac{1}{h_0} z_* \,,\; x = \dfrac{1}{h_0} x_* \,,\; \psi = \dfrac{1}{UL}\psi_* \\ \omega = \dfrac{h_0}{U}\omega_* \,,\; T = \dfrac{1}{T_0} T_* \end{cases} \tag{2}$$

$$\begin{cases} \dfrac{\partial\psi}{\partial z}\dfrac{\partial\omega}{\partial x}-\dfrac{\partial\psi}{\partial x}\dfrac{\partial\omega}{\partial z}+\alpha\dfrac{\partial T}{\partial x}=\varepsilon\left(\dfrac{\partial^2\omega}{\partial x^2}+\dfrac{\partial^2\omega}{\partial z^2}\right) \\ k\omega=\dfrac{\partial^2\psi}{\partial x^2}+\dfrac{\partial^2\psi}{\partial z^2} \\ \dfrac{\partial\psi}{\partial z}\dfrac{\partial T}{\partial x}-\dfrac{\partial\psi}{\partial x}\dfrac{\partial T}{\partial z}-A\dfrac{\partial\psi}{\partial x}=\dfrac{\varepsilon}{\mathrm{Pr}}\left(\dfrac{\partial^2 T}{\partial x^2}+\dfrac{\partial^2 T}{\partial z^2}\right) \end{cases} \tag{3}$$

$$\begin{cases} k=\dfrac{h_0}{L},\ \mathrm{Pr}=\dfrac{\nu}{\kappa} \\ \alpha=\dfrac{\alpha g T_0 h_0}{U^2},\ \varepsilon=\dfrac{\nu}{UL} \end{cases} \tag{4}$$

temperature lapse rate; x and z = dimensionless horizontal and vertical axes, respectively; h_0 = height of cold air flow along the coast; U = upper wind velocity; L = distance of an extended cold air flow; T_0 = temperature difference between a cold air flow and air over the sea; Pr = Prandtl number; and ε = the reciprocal of Reynold's number.

The perturbation equation is shown in Eq. 5, from which Eqs. 6-8 are obtained.

Perturbation Eq. :

$$\begin{cases} \psi=\psi_0+k\psi_1+k^2\psi_2+\cdots \\ \omega=\omega_0+k\omega_1+k^2\omega_2+\cdots \\ T=T_0+kT_1+k^2T_2+\cdots \end{cases} \tag{5}$$

Zero-order Eq. :

$$\begin{cases} \dfrac{\partial\psi_0}{\partial z}\dfrac{\partial\omega_0}{\partial x}-\dfrac{\partial\psi_0}{\partial x}\dfrac{\partial\omega_0}{\partial z}=\varepsilon\left(\dfrac{\partial^2\omega_0}{\partial x^2}+\dfrac{\partial^2\omega_0}{\partial z^2}\right) \\ 0=\dfrac{\partial^2\psi_0}{\partial x^2}+\dfrac{\partial^2\psi_0}{\partial z^2} \\ \dfrac{\partial\psi_0}{\partial z}\dfrac{\partial T_0}{\partial x}-\dfrac{\partial\psi_0}{\partial x}\dfrac{\partial T_0}{\partial z}-A\dfrac{\partial\psi_0}{\partial x}=\dfrac{\varepsilon}{\mathrm{Pr}}\left(\dfrac{\partial^2 T_0}{\partial x^2}+\dfrac{\partial^2 T_0}{\partial z^2}\right) \end{cases} \tag{6}$$

First-order Eq. :

$$\begin{cases} \dfrac{\partial\psi_1}{\partial z}\dfrac{\partial\omega_0}{\partial x}-\dfrac{\partial\psi_1}{\partial x}\dfrac{\partial\omega_0}{\partial z}+\dfrac{\partial\psi_0}{\partial z}\dfrac{\partial\omega_1}{\partial x}-\dfrac{\partial\psi_0}{\partial x}\dfrac{\partial\omega_1}{\partial z}+\alpha\dfrac{\partial T_0}{\partial x}=\varepsilon\left(\dfrac{\partial^2\omega_1}{\partial x^2}+\dfrac{\partial^2\omega_1}{\partial z^2}\right) \\ \omega_0=\dfrac{\partial^2\psi_1}{\partial x^2}+\dfrac{\partial^2\psi_1}{\partial z^2} \\ \dfrac{\partial\psi_1}{\partial z}\dfrac{\partial T_0}{\partial x}-\dfrac{\partial\psi_1}{\partial x}\dfrac{\partial T_0}{\partial z}+\dfrac{\partial\psi_0}{\partial z}\dfrac{\partial T_1}{\partial x}-\dfrac{\partial\psi_0}{\partial x}\dfrac{\partial T_1}{\partial z}-A\dfrac{\partial\psi_1}{\partial x}=\dfrac{\varepsilon}{\mathrm{Pr}}\left(\dfrac{\partial^2 T_1}{\partial x^2}+\dfrac{\partial^2 T_1}{\partial z^2}\right) \end{cases} \tag{7}$$

Second-order Eq. :

$$\begin{cases} \dfrac{\partial\psi_2}{\partial z}\dfrac{\partial\omega_0}{\partial x}-\dfrac{\partial\psi_2}{\partial x}\dfrac{\partial\omega_0}{\partial z}+\dfrac{\partial\psi_1}{\partial z}\dfrac{\partial\omega_1}{\partial x}-\dfrac{\partial\psi_1}{\partial x}\dfrac{\partial\omega_1}{\partial z}+\dfrac{\partial\psi_0}{\partial z}\dfrac{\partial\omega_2}{\partial x}-\dfrac{\partial\psi_0}{\partial x}\dfrac{\partial\omega_2}{\partial z}+\alpha\dfrac{\partial T_1}{\partial x}=\varepsilon\left(\dfrac{\partial^2\omega_2}{\partial x^2}+\dfrac{\partial^2\omega_2}{\partial z^2}\right) \\ \omega_1=\dfrac{\partial^2\psi_2}{\partial x^2}+\dfrac{\partial^2\psi_2}{\partial z^2} \\ \dfrac{\partial\psi_2}{\partial z}\dfrac{\partial T_0}{\partial x}-\dfrac{\partial\psi_2}{\partial x}\dfrac{\partial T_0}{\partial z}+\dfrac{\partial\psi_1}{\partial z}\dfrac{\partial T_1}{\partial x}-\dfrac{\partial\psi_1}{\partial x}\dfrac{\partial T_1}{\partial z}+\dfrac{\partial\psi_0}{\partial z}\dfrac{\partial T_2}{\partial x}-\dfrac{\partial\psi_0}{\partial x}\dfrac{\partial T_2}{\partial z}-A\dfrac{\partial\psi_2}{\partial x}=\dfrac{\varepsilon}{\mathrm{Pr}}\left(\dfrac{\partial^2 T_2}{\partial x^2}+\dfrac{\partial^2 T_2}{\partial z^2}\right) \end{cases} \tag{8}$$

Using green function theory the following solutions (Eqs. 9-18) are derived. (1) Zero-order Eq. 6: A stream function is derived by potential flow. Vorticity is equal to zero. T is determined under a potential flow with consideration given to the temperature difference between the cold air flow and air over the sea. (2) First-order Eq. 7: A stream function and T are equal to 0 ℃. Vorticity is affected by T of zero order in Eq. 6. (3) Second-order Eq. 8: A stream function is derived considering the effect of the vorticity of the first-order Eq. 7. Vorticity is equal to zero. T is the temperature distribution but its effect is very small, therefore T is neglected.

We assumed that the potential flow is greatly affected by the shape of the cold

air flow. The potential flow is therefore obtained by orthogonal axis transformation. However, with regards to T of zero-order Eq. 6, T is caused by only the temperature difference between the cold air flow and the air over the sea. Therefore, the shape effect of the cold air flow is neglected as the effect is smaller than the temperature difference. The vorticity of first-order Eq. 7 is obtained by the green function theory, and it is approximated in Eq. 15 because it is easier to solve the stream function of second-order Eq. 8.

Zero-order solutions :

$$\psi_0(\bar{x},\bar{z}) = \bar{z} - \frac{\bar{z}}{\bar{x}^2+\bar{z}^2} \qquad \begin{cases} x = \bar{x} + \dfrac{a^2\bar{x}}{\bar{x}^2+\bar{y}^2} \\ y = \bar{y} - \dfrac{a^2\bar{y}}{\bar{x}^2+\bar{y}^2} \end{cases} \tag{9}$$

$$\omega_0(x,z) = 0 \tag{10}$$

$$T_0 = \alpha u_0 \left\{ -\frac{1}{2l} e^{-il(R+\xi-i\eta)} \mathrm{Ei}\left[il(R+\xi-i\eta) - lz_0\right] - \frac{1}{2l} e^{il(R+\xi+i\eta)} \mathrm{Ei}\left[-il(R+\xi+i\eta) - lz_0\right] \right.$$
$$+ \frac{1}{l} e^{-lz_0} \log\left[\sqrt{(\xi+R)^2+(\eta-z_0)^2}\right] - \frac{1}{2l} e^{-il(R+\xi-i\eta)} \mathrm{Ei}\left[-il(R+\xi-i\eta) - lz_0\right] \qquad \mathrm{Ei}[z] = -\int_{-z}^{\infty} \frac{e^{-t}}{t} dt$$
$$\left. - \frac{1}{2l} e^{il(R+\xi+i\eta)} \mathrm{Ei}\left[il(R+\xi+i\eta) - lz_0\right] + \frac{1}{l} e^{-lz_0} \log\left[\sqrt{(\xi+R)^2+(\eta+z_0)^2}\right] \right\} \tag{11}$$

First-order solutions :

$$\psi_1(x,z) = 0 \tag{12}$$

$$\omega_1 = \alpha a \varepsilon^3 \left\{ -\frac{1}{2l} e^{-il(R+\xi-i\eta)} \mathrm{Ei}\left[il(R+\xi-i\eta) - lz_0\right] - \frac{1}{2l} e^{il(R+\xi+i\eta)} \mathrm{Ei}\left[-il(R+\xi+i\eta) - lz_0\right] \right.$$
$$+ \frac{1}{l} e^{-lz_0} \log\left[\sqrt{(\xi+R)^2+(\eta-z_0)^2}\right] - \frac{1}{2l} e^{-il(R+\xi-i\eta)} \mathrm{Ei}\left[-il(R+\xi-i\eta) - lz_0\right]$$
$$\left. - \frac{1}{2l} e^{il(R+\xi+i\eta)} \mathrm{Ei}\left[il(R+\xi+i\eta) - lz_0\right] + \frac{1}{l} e^{-lz_0} \log\left[\sqrt{(\xi+R)^2+(\eta+z_0)^2}\right] \right\} \tag{13}$$

$$T_1(x,z) = 0 \tag{14}$$

$$\omega_1 = -e^{-a|x-x_0|} \cos\left\{b(z-z_0)\right\} \tag{15}$$

$$-\infty \le x \le \infty$$

$$-\frac{\pi}{2} \le b(z-z_0) \le \frac{\pi}{2}$$

Second-order solutions :

$$\psi_2 = \frac{1}{b^2-a^2} e^{-a|x-x_0|} \cos\left\{b(z-z_0)\right\} \tag{16}$$

$$\omega_2(x,z) = 0 \tag{17}$$

$$T_2(x,z) = 0 \tag{18}$$

where α = coefficient of Heaviside function; a1,b = coefficients of the approximation of the green function; l(= Cf U/(2 k) h0/T0) = coefficient of the thermal transmission obtained by the Bulk coefficient; Cf = Bulk coefficient; z_0 = center of vorticity in the z direction; R,x_0 = front edge of an extended cold air flow in the x direction; x = $x/\varepsilon^{1/2}$; and h = $z/\varepsilon^{1/2}$. The values of a, A and k are obtained from Table 2. Fig. 2 shows the boundary condition around Ishikari Bay in winter.

Table 1 Conditions of the calculations

case	ν(m^2/sec)	Pr	Fig.
case 1	300.0	1.0	Fig. 3
case 2	1000.0	0.5	Fig. 4
case 3	1000.0	1.0	Fig. 5
case 4	1000.0	2.0	Fig. 6

Fig. 3 - Fig. 6 show the results of calculations by changing the values of ν and Pr in Table 1. In these figures, the vector is normalized by h_0/U/L and vorticity is

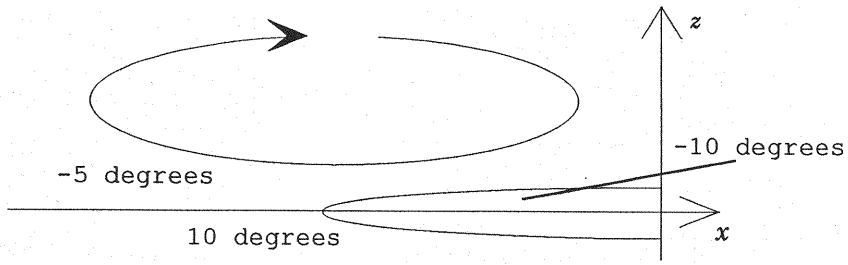

Fig. 2 Boundary condition of the horizontal convection

Table 2 Conditions of the calculations

$U = 8\ m/s$	$h_0 = 500\ m$	(19)
$\alpha = 0.0036643\ 1/℃$	$L = 5{,}000\ m$	
$g = 9.8\ m/s^2$	$T_0 = 20\ ℃$	
$\Gamma = 1/100\ ℃/m$		

$$a = \frac{\alpha g T_0 h_0}{U^2} = \frac{0.0036643 \times 9.8 \times 20 \times 500}{8^2} = 5.611 \qquad (20)$$

$$A = \frac{\Gamma h_0}{T_0} = \frac{-0.02 \times 500}{20} = 0.50 \qquad (20)$$

$$k = \frac{h_0}{L} = \frac{500}{5000} = 0.10 \qquad (20)$$

normalized by h_0/U. Case 1 and case 3: In case 1 the wind field is similar to the potential flow because vorticity is too small to affect the vector. Although Pr is the same value in both case 1 and case 3, the horizontal convection effect is only shown in case 3. When ν is approximately 300 m^2/sec, the horizontal convection effect is small. The center of vorticity in case 1 is lower than that in case 3, and the vorticity in case 3 is greater than that in case 1. These results show that the greater the viscosity is, the greater the vorticity and the higher the center of vorticity become. Case 2 - case 4: Viscosity is the same value and the Pr number is changed from 0.5 to 2.0. The smaller the Pr number is, the higher the center of vorticity becomes. A smaller Pr number means that the thermal diffusivity increases, and a greater thermal diffusivity indicates an increase in the scale of vorticity. In general, the wind field is not changed by horizontal convection as long as the viscosity is not high.

Unsteady wind field

In the steady wind field section, it was found that the wind field is not affected by horizontal convection. Therefore, we conclude that an unsteady wind field simply. Eq. 23 shows a dimensionless equation obtained from Eq. 22:

$$\begin{cases} \dfrac{\partial \omega_*}{\partial t_*} + \dfrac{\partial \psi_*}{\partial z_*}\dfrac{\partial \omega_*}{\partial x_*} - \dfrac{\partial \psi_*}{\partial x_*}\dfrac{\partial \omega_*}{\partial z_*} + \alpha g \dfrac{\partial T_*}{\partial x_*} = \nu\left(\dfrac{\partial^2 \omega_*}{\partial x_*^{\,2}} + \dfrac{\partial^2 \omega_*}{\partial z_*^{\,2}}\right) \\ \omega_* = \dfrac{\partial^2 \psi_*}{\partial x_*^{\,2}} + \dfrac{\partial^2 \psi_*}{\partial z_*^{\,2}} \\ \dfrac{\partial T_*}{\partial t_*} + \dfrac{\partial \psi_*}{\partial z_*}\dfrac{\partial T_*}{\partial x_*} - \dfrac{\partial \psi_*}{\partial x_*}\dfrac{\partial T_*}{\partial z_*} - \Gamma \dfrac{\partial \psi_*}{\partial x_*} = \kappa\left(\dfrac{\partial^2 T_*}{\partial x_*^{\,2}} + \dfrac{\partial^2 T_*}{\partial z_*^{\,2}}\right) \end{cases} \qquad (21)$$

$$\begin{cases} z = \dfrac{1}{h_0} z_*\ ,\ x = \dfrac{1}{h_0} x_*\ ,\ \psi = \dfrac{1}{UL}\psi_* \\ \omega = \dfrac{h_0}{U}\omega_*\ ,\ T = \dfrac{1}{T_0} T_*\ ,\ t = \dfrac{UL}{h_0^{\,2}} t_* \end{cases} \qquad (22)$$

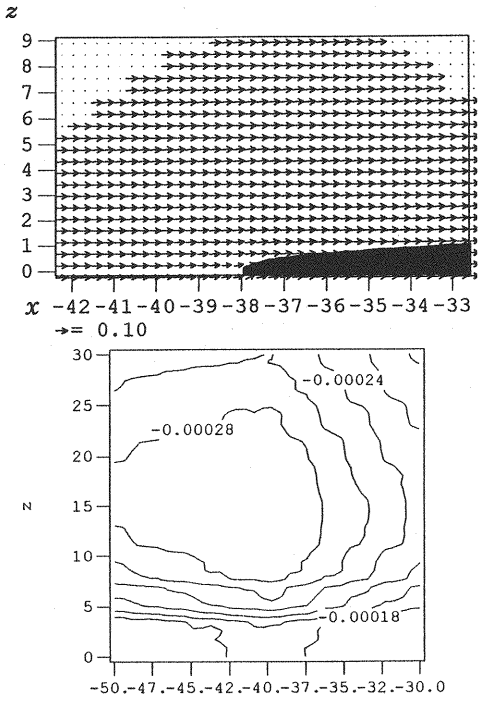

Fig. 3 Case1 vector and viscosity

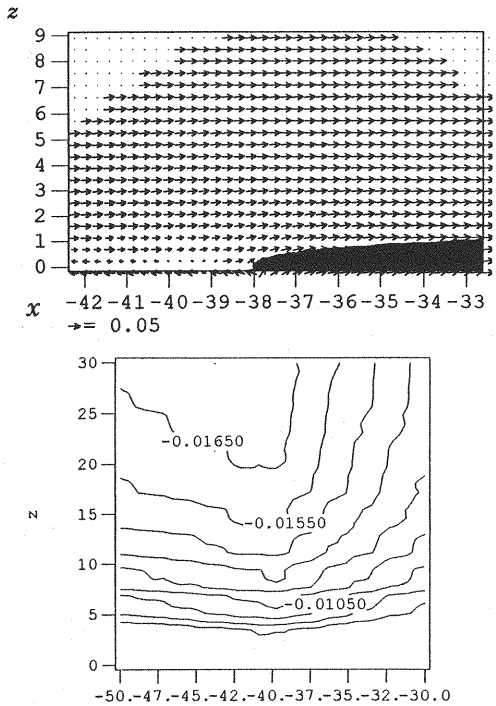

Fig. 4 Case2 vector and viscosity

These wind fields are subtracted Ψ_0

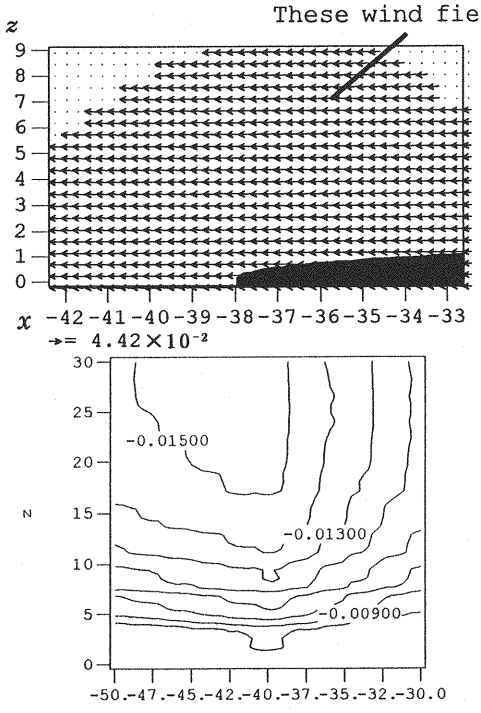

Fig. 5 Case3 vector and viscosity

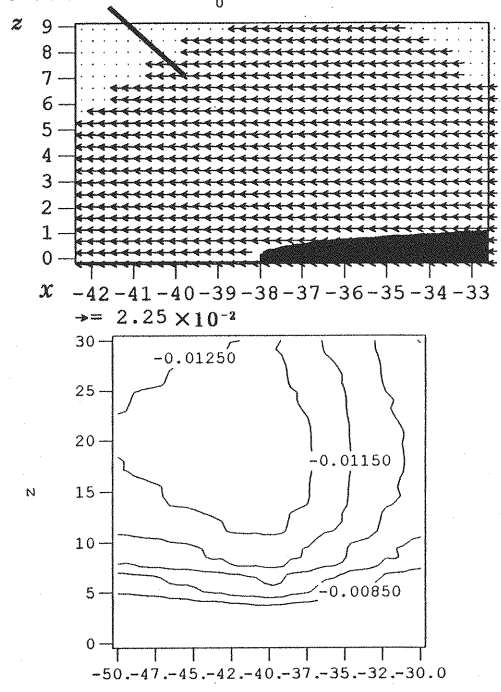

Fig. 6 Case4 vector and viscosity

$$\begin{cases} \dfrac{\partial\omega}{\partial t}+\dfrac{\partial\psi}{\partial z}\dfrac{\partial\omega}{\partial x}-\dfrac{\partial\psi}{\partial x}\dfrac{\partial\omega}{\partial z}+a\dfrac{\partial T}{\partial x}=\varepsilon\left(\dfrac{\partial^2\omega}{\partial x^2}+\dfrac{\partial^2\omega}{\partial z^2}\right) \\ k\omega=\dfrac{\partial^2\psi}{\partial x^2}+\dfrac{\partial^2\psi}{\partial z^2} \\ \dfrac{\partial T}{\partial t}+\dfrac{\partial\psi}{\partial z}\dfrac{\partial T}{\partial x}-\dfrac{\partial\psi}{\partial x}\dfrac{\partial T}{\partial z}-A\dfrac{\partial\psi}{\partial x}=\dfrac{\varepsilon}{\mathrm{Pr}}\left(\dfrac{\partial^2 T}{\partial x^2}+\dfrac{\partial^2 T}{\partial z^2}\right) \end{cases} \tag{23}$$

$$\begin{cases} k=\dfrac{h_0}{L},\ \mathrm{Pr}=\dfrac{\nu}{\kappa} \\ a=\dfrac{\alpha g T_0 h_0}{U^2},\ \varepsilon=\dfrac{\nu}{UL} \end{cases} \tag{24}$$

where t = dimensionless time.

The perturbation equation is shown by Eq. 25. Under the boundary condition, the temperature of the sea changes by a daytime cycle $T = T_0 \sin(\omega t)$. The solutions of Eq. 25 are shown in Eqs. 26-34.

Perturbation Eq. :

$$\begin{cases} \psi=\psi_0+k\psi_1+k^2\psi_2+\cdots \\ \omega=\omega_0+k\omega_1+k^2\omega_2+\cdots \\ T=T_0+kT_1+k^2T_2+\cdots \end{cases} \tag{25}$$

Zero-order solutions :

$$\psi_0(\bar{x},\bar{z})=\bar{z}-\frac{\bar{z}}{\bar{x}^2+\bar{z}^2} \qquad \begin{cases} x=\bar{x}+\dfrac{a^2\bar{x}}{\bar{x}^2+\bar{y}^2} \\ y=\bar{y}-\dfrac{a^2\bar{y}}{\bar{x}^2+\bar{y}^2} \end{cases} \tag{26}$$

$$\omega_0(x,z)=0 \tag{27}$$

$$T_0=\sin\left(\omega_* t+\gamma-\sqrt{\frac{\varepsilon\omega_*}{2\mathrm{Pr}}}z\right)\times\exp\left(-\sqrt{\frac{\varepsilon\omega_*}{2\mathrm{Pr}}}z\right)(Ts-Tc)\left[u(-x-x_a)+u(x-x_a)\right]+\frac{\varepsilon}{\mathrm{Pr}}\iint\frac{u_0\alpha(Ts-Tc)}{4\pi}\frac{u[t-t']}{t-t'}$$

$$\left[-\sin\left(\omega_* t'+\gamma-\sqrt{\frac{\varepsilon\omega_*}{2\mathrm{Pr}}}z\right)\exp\left(-\sqrt{\frac{\varepsilon\omega_*}{2\mathrm{Pr}}}z\right)\left\{\exp\left(-\frac{\mathrm{Pr}}{\varepsilon}\frac{\left(-x_R-x'\right)^2+(z-z')^2}{4(t-t')}\right)-\exp\left(-\frac{\mathrm{Pr}}{\varepsilon}\frac{\left(-x_R-x'\right)^2+(z-z')^2}{4(t-t')}\right)\right\}\right.$$

$$\left.+\sin\left(\omega_* t'+\gamma-\sqrt{\frac{\varepsilon\omega_*}{2\mathrm{Pr}}}z\right)e^{-\sqrt{\frac{\varepsilon\omega_*}{2\mathrm{Pr}}}z}\left\{\exp\left(-\frac{\mathrm{Pr}}{\varepsilon}\frac{\left(x_R-x'\right)^2+(z-z')^2}{4(t-t')}\right)-\exp\left(-\frac{\mathrm{Pr}}{\varepsilon}\frac{\left(x_R-x'\right)^2+(z-z')^2}{4(t-t')}\right)\right\}\right]dzdt \tag{28}$$

$$\omega=\delta^{\frac{3}{2}}\omega_*,\ \delta=\left(\frac{\varepsilon}{\mathrm{Pr}}\right)^2$$

First-order solutions :

$$\psi_1(x,z)=0 \tag{29}$$

$$\omega_1=\varepsilon^3\iint\frac{a\alpha(Ts-Tc)}{4\pi}\frac{u[t-t']}{t-t'}$$

$$\left[-\sin\left(\omega_* t'+\gamma-\sqrt{\frac{\varepsilon\omega_*}{2\mathrm{Pr}}}z\right)\exp\left(-\sqrt{\frac{\varepsilon\omega_*}{2\mathrm{Pr}}}z\right)\left\{\exp\left(-\frac{\mathrm{Pr}}{\varepsilon}\frac{\left(-x_R-x'\right)^2+(z-z')^2}{4(t-t')}\right)-\exp\left(-\frac{\mathrm{Pr}}{\varepsilon}\frac{\left(-x_R-x'\right)^2+(z-z')^2}{4(t-t')}\right)\right\}\right.$$

$$\left.+\sin\left(\omega_* t'+\gamma-\sqrt{\frac{\varepsilon\omega_*}{2\mathrm{Pr}}}z\right)\exp\left(-\sqrt{\frac{\varepsilon\omega_*}{2\mathrm{Pr}}}z\right)\left\{\exp\left(-\frac{\mathrm{Pr}}{\varepsilon}\frac{\left(x_R-x'\right)^2+(z-z')^2}{4(t-t')}\right)-\exp\left(-\frac{\mathrm{Pr}}{\varepsilon}\frac{\left(x_R-x'\right)^2+(z-z')^2}{4(t-t')}\right)\right\}\right]dzdt \tag{30}$$

$$T_1(x,z)=0 \tag{31}$$

$$\omega_1=-e^{-a|x-x_0|}\cos\left\{\frac{\pi}{2b}(z-z_0)\right\}\times B$$

$$b=a_0+a_1\ln(time)$$

$$B=a_2\sin(\omega\cdot time+a_3)$$

$$a=a_4+a_5t+a_6t^2+a_7t^3+a_8t^4$$

Second-order solutions :

$$\psi_2=\frac{B}{b^2-a^2}e^{-a|x-x_0|}\cos\left\{b(z-z_0)\right\} \tag{32}$$

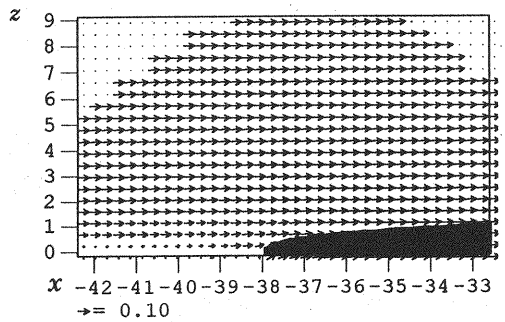

Fig. 7 Vector on the maximum vorticity

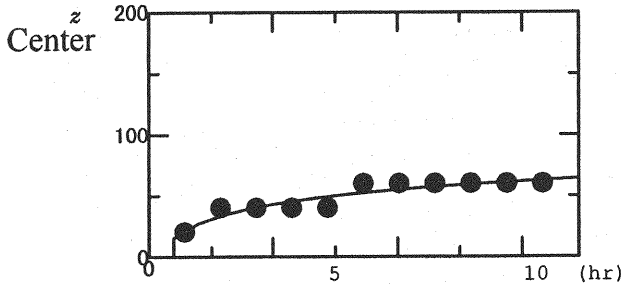

Fig. 8 Center of the vorticity

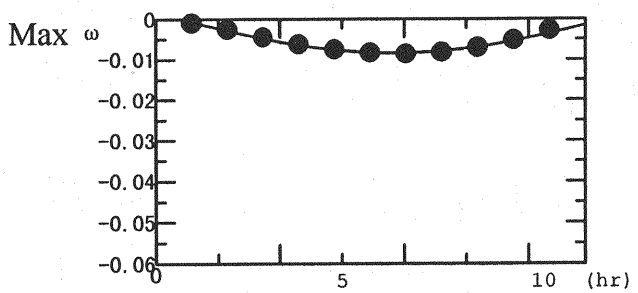

Fig. 9 Strength of the maximum vorticity

$$\omega_2(x,z) = 0 \tag{33}$$

$$T_2(x,z) = 0 \tag{34}$$

where a0 - a8 = coefficients of the approximation of the green function.

Fig. 7 shows the vector around the cold air flow. The wind field is greatly affected by the potential flow. Thus, this result is similar to that obtained for the steady state. Fig. 8 and Fig. 9 show the calculated location of the center of the vorticity and the strength of maximum vorticity, respectively, under the conditions that ν = 3000.0 m^2/sec and Pr = 1.0. Other conditions are the same as those in the steady wind field calculations. In Fig. 8, the center of the vorticity increases with time. In Fig. 9, the temperature of the sea changes by a daily cycle and the maximum temperature difference is at 6 hr. The maximum strength of the maximum vorticity is caused at 6:50. The greater the vorticity is, the easier it is for snow clouds to form. Therefore a convection occurs easily when the difference in temperature is maximum. Other results, for example the changes in ν and Pr, are the same.

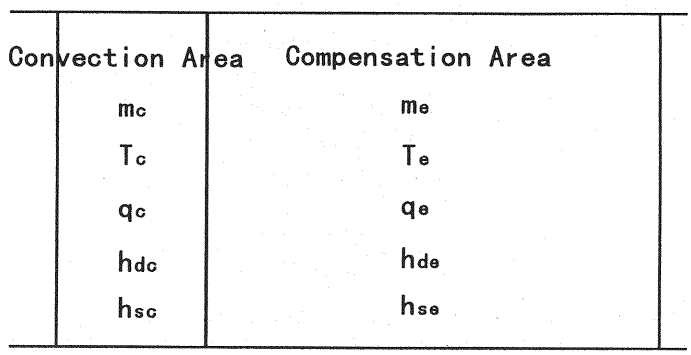

Fig. 10 Cumulus convection model

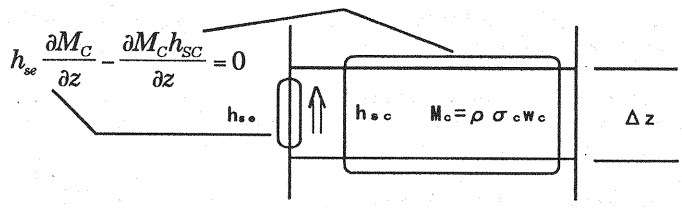

Fig. 11 Continuity of the moist energy

CUMULUS CONVECTION MODEL WITH AN ASCENDING WIND

The results of horizontal convection showed the temperature difference between the cold air flow and the sea is not related to the convection around the cold air flow. Many observations have shown that an ascending wind at the edge of a cold air flow plays an important role in the formation of snow clouds. In this section, it is assumed that a cumulus convection is caused by an ascending wind, and the wind field is analyzed using it. This model is a very simple one as it has only two areas: a cumulus convection area and a compensation area. It imitates a cumulus convection using an entrain and a detrain. The relationship between vapor and cloud water is parameterized, then analytical solutions are obtained.

Cumulus convection model (1)

Fig. 10 shows the cumulus convection model, where T = temperature; q = specific humidity; hd(= C_P T + g z) = energy of dry air; hs(= C_P T + g z + l q) = energy of moist air; The subscriptions c and e mean cumulus convection area and a compensation area, respectively. Fig. 11 shows a continuity of the moist energy. The equation in Fig. 11 is divided into two equations: Eq. 35 and Eq. 36. These equations show that energy in dry air is obtained by condensing vapor and freezing cloud water, and the vapor is decreased by condensing it.

$$h_{dL}\frac{\partial M_C}{\partial t}-\frac{\partial M_C h_{dC}}{\partial x}+\rho L(C-E)=0 \tag{35}$$

$$q_L\frac{\partial M_C}{\partial t}-\frac{\partial M_C q_C}{\partial x}-\rho(C-E)=0 \tag{36}$$

Eqs. 37 - 39 show the momentum equation, the first law of thermodynamics, and the continuity equation, respectively.

$$\frac{\partial w_*}{\partial t_*}+w_*\frac{\partial w_*}{\partial z_*}=-\frac{1}{\rho}\frac{\partial p}{\partial z_*}-g=\frac{T_{ve^*}-T_{ve^*}}{T_{ve^*}}g \tag{37}$$

$$\frac{\partial \theta_*}{\partial t_*}+w_*\frac{\partial \theta_*}{\partial z_*}=\frac{\theta_*}{C_P T_*}L(C-E) \tag{38}$$

$$h_{dL}\frac{\partial M_c}{\partial z}-\frac{\partial M_c h_{dc}}{\partial z}+\rho L(C-E)=0 \tag{39}$$

$$\left.\begin{aligned} h_{dL} &= C_P T_{L*}+gz_* \\ M_c &= \rho\sigma_c w_{c*} \\ h_{dc} &= C_P T_{c*}+gz_* \end{aligned}\right\} \tag{40}$$

$$\theta_* = T_*\left(\frac{p_0}{p}\right)^{\frac{Rd}{C_P}} \tag{41}$$

where σ_C = ratio of a convection area to the total area; w_* = velocity in the z direction; t_* = potential temperature; p = pressure; g = 9.8 m/sec^2; T_{VC*} = virtual temperature in a convection area; T_{Ve*} = virtual temperature in a compensation area; T_* = temperature; C_P = specific heat; L = latent heat of condensation; C = condensation ratio of the vapor; E = evaporation of cloud water; R_d = gas constant; T_M = temperature difference between the cold air flow and the sea; Ti = 1000 sec; h_M = 4000 m; and w_M = convergence wind.

Explanation for the equations is following. (1) Momentum Eq. 37: This is affected by the temperature considering the vertical component only. It is assumed that the vertical pressure profile in the convection area agrees with that in the compensation area and that they are in a hydrostatic equilibrium, because the height of a cumulus convection that appears around Ishikari Bay is lower than usual. (2) First law of thermodynamics Eq. 38: This considers the change from vapor to cloud water and the evaporation from cloud water to vapor. (3) Continuity of energy Eq. 39: This includes an entrain and a detrain. It is possible to estimate a specific humidity by considering the adiabatic process in a convection area.

We can obtain a cumulus convection model by substituting the ratio of non-adiabatic heat given in Eq. 39 into the first law of thermodynamics Eq. 38. With regard to boundary conditions, the components in a compensation area maintain constant values, and an ascending wind generated at the edge of a cold air flow in the area below the convection area.

$$\begin{aligned} \theta_* &= T_M\theta \ , \ t_* = T_i t \\ z_* &= h_M z \ , \ w_{c*} = w_M w_c \end{aligned} \tag{42}$$

Eq. 43 is obtained from Eqs. 37 - 42.

$$\left\{\begin{aligned} &\eta\frac{\partial\theta_c}{\partial t}+w_c\frac{\partial\theta_c}{\partial z}=-\varphi\theta_L\frac{\partial w_c}{\partial z}+\varphi\frac{\partial\theta_c w_c}{\partial z}+\varphi b\theta_c w_c+\varphi a w_c \\ &\theta_c=\theta_X\varepsilon^2\frac{\partial w_c}{\partial t}+\zeta\theta_X w_c\frac{\partial w_c}{\partial z}+\theta_a+\theta_K \end{aligned}\right. \tag{43}$$

$$\varphi=\sigma_c \ , \ b=\frac{Rd}{C_P}\frac{\partial\ln p}{\partial z} \ , \ a=\frac{gh_M}{T_M C_P}\left(\frac{p_0}{p}\right)^{\frac{Rd}{C_P}}$$

Basic Eq. 45 is given using Eq. 44.

$$t=\varepsilon\tau \tag{44}$$

$$\left\{\begin{aligned} &\frac{\eta}{\varepsilon}\frac{\partial\theta_c}{\partial\tau}+w_c\frac{\partial\theta_c}{\partial z}=-\varphi\theta_L\frac{\partial w_c}{\partial z}+\varphi\frac{\partial\theta_c w_c}{\partial z}+\varphi b\theta_c w_c+\varphi a w_c \\ &\theta_c=\theta_X\varepsilon\frac{\partial w_c}{\partial\tau}+\zeta\theta_X w_c\frac{\partial w_c}{\partial z}+\theta_a+\theta_K \end{aligned}\right. \tag{45}$$

$$\eta=\frac{h_M}{T_i w_M} \ , \ \varphi=\sigma_c \ , \ b=\frac{Rd}{C_P}\frac{\partial\ln p}{\partial z}$$

$$a=\frac{gh_M}{T_M C_P}\left(\frac{p_0}{p}\right)^{\frac{Rd}{C_P}} \ , \ \varepsilon=\frac{w_M}{gT_i} \ , \ \zeta=\frac{w_M^2}{gh_M} \tag{46}$$

$$z=18410.0\log_{10}\frac{1013.25}{p}\Rightarrow p=\frac{1013.25}{10^{z/18410.0}}$$

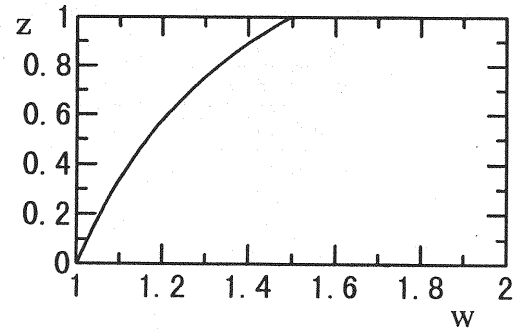

Fig. 12 Vertical wind velocity profile

w_c is assumed as in Eq. 47 by considering that an initial ascending wind that is generated at the edge of a cold air flow. Eqs. 49 - 52 are obtained by perturbation Eq. 48.

$$w_c = w_X + w_e \tag{47}$$

Perturbation Eq. :

$$w_e = w_{000} + \varepsilon w_{001} + \frac{\zeta}{\varepsilon} w_{010} + \zeta w_{011} + \varepsilon^2 w_{002} + \left(\frac{\zeta}{\varepsilon}\right)^2 w_{020} + \cdots$$

$$+ b\left(w_{100} + \varepsilon w_{101} + \frac{\zeta}{\varepsilon} w_{110} + \cdots\right) \tag{48}$$

Zero-order Eq. :

$$\eta\theta_X \frac{\partial^2 w_{000}}{\partial \tau^2} + \left(w_X + w_{000}\right)\frac{\partial \theta_\alpha}{\partial z} = \varphi w_X \frac{\partial \theta_\alpha}{\partial z} + \varphi a w_X \tag{49}$$

Zero-order Eq. of b :

$$\eta\theta_X \frac{\partial^2 w_{100}}{\partial \tau^2} + w_{100}\frac{\partial \theta_\alpha}{\partial z} = \varphi w_X \left(\theta_\alpha + \theta_K\right) \tag{50}$$

Zero-order solution :

$$w_{000} = w_X\left\{-1 + \varphi\left(1 + \frac{a}{\partial\theta_\alpha/\partial z}\right)\right\} + c_1 \sin\left(\sqrt{\frac{1}{\eta\theta_X}\frac{\partial\theta_\alpha}{\partial z}}\tau\right) + c_2 \cos\left(\sqrt{\frac{1}{\eta\theta_X}\frac{\partial\theta_\alpha}{\partial z}}\tau\right) \tag{51}$$

Zero-order solution of b :

$$w_{100} = \varphi\frac{\theta_\alpha + \theta_K}{\partial\theta_\alpha/\partial z} w_X + c_3 \sin\left(\sqrt{\frac{1}{\eta\theta_X}\frac{\partial\theta_\alpha}{\partial z}}\tau\right) + c_4 \cos\left(\sqrt{\frac{1}{\eta\theta_X}\frac{\partial\theta_\alpha}{\partial z}}\tau\right) \tag{52}$$

In perturbation Eq. 47, the effects of first- and second-order solutions like w001 and w010 are much smaller than the zero-order solution, therefore they are therefore neglected. If an ascending wind below the convection area has constant w_x over time, c1=0, c2=0, c3=0 and c4=0 is obtained and ψ is determined by the boundary condition of $w_c|_{z=0} = w_x$. (Eq. 53)

$$w_c = w_X + w_X\left\{-1 + \varphi\left(1 + \frac{a}{\partial\theta_\alpha/\partial z}\right)\right\} + b\varphi\frac{\theta_\alpha + \theta_K}{\partial\theta_\alpha/\partial z} w_X$$

$$= \varphi\left\{1 + \frac{1}{\partial\theta_\alpha/\partial z}\left[a + b\left(\theta_\alpha + \theta_K\right)\right]\right\} w_X$$

$$w_c|_{z=0} = w_X$$

$$\downarrow$$

$$\varphi = 1\Big/\left\{1 + \frac{1}{\partial\theta_\alpha/\partial z}\left[a + b\left(\theta_\alpha + \theta_K\right)\right]\right\}\Big|_{z=0} \tag{53}$$

Application to actual phenomena

Table 3 shows an example of a case in which convergence band clouds appeared

Table 3 Conditions of the calculations

$$\left.\begin{array}{ll} h_M = 4000\,m & Rd = 289\,m^2/s^2K \\ w_M = 1\,m/s & C_P = 1006\,m^2/s^2K \\ T_i = 1000\,sec & T_M = 10\,℃ \end{array}\right\} \quad (54)$$

around Ishikari Bay. The vertical temperature profile is given by radiosonde data. $\sigma_c = \psi$ is 0.254 obtained by Eq. 53. Fig. 12 shows the vertical wind velocity using Eqs. 47 - 52. The wind velocity derived from the entrainment of energy in the compensation area. This phenomenon is found in the developmental stage of a cumulus convection.

Low pressure over Ishikari Bay area

Snow clouds accompanying a cold air flow may change from convective clouds to low pressure over Ishikari Bay area because of the strength of its convection. In Fig. 13 and Fig. 14, radar refrectivity show a convergence band cloud and low pressure over Ishikari Bay area on Jan. 7, 1996 and on Jan. 8, 1996, respectively. (The snow cloud in Fig. 13, however, is not thought to be one accompanying a cold air flow.) After 3 hours, the convective band cloud changed into low pressure over the Ishikari Bay area. The center of the low-pressure zone was located over Otaru, and the horizontal eddy is shown. On Jan. 8, 1996 Otaru had the heaviest snowfall in 35 years.

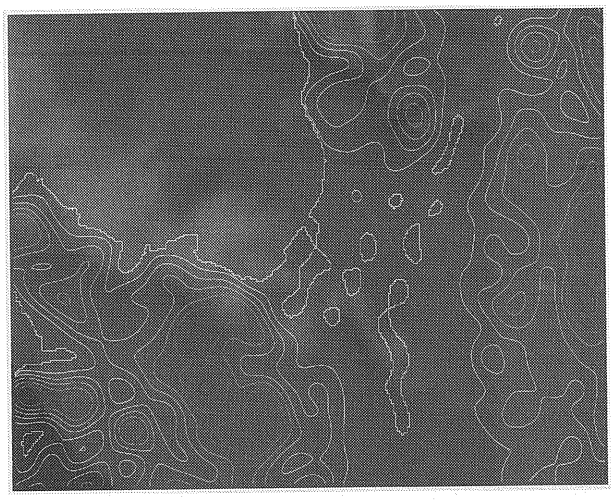

Fig. 13 Radar refrectivity on Jan. 7, 1996 at 23:00

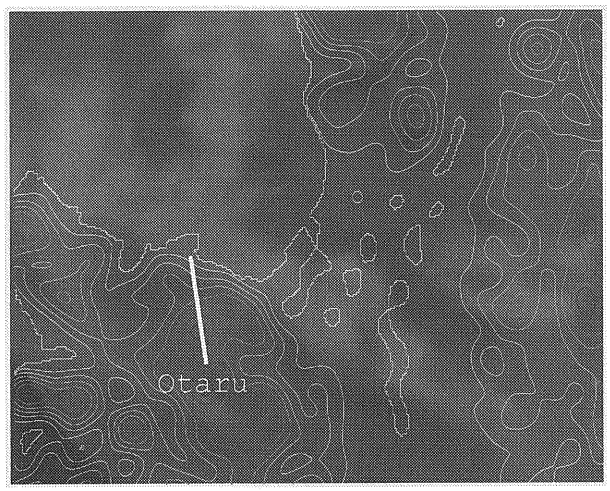

Fig. 14 Radar refrectivity on Jan. 8, 1996 at 2:00

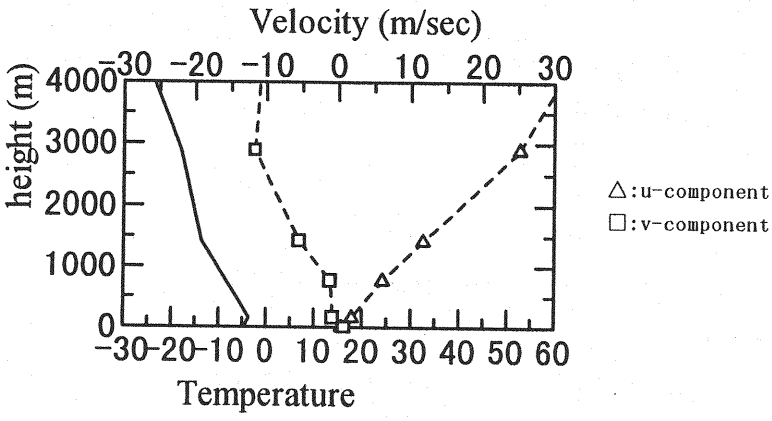

Fig. 15 Radiosonde data at 21:00 on Jan. 7, 1996

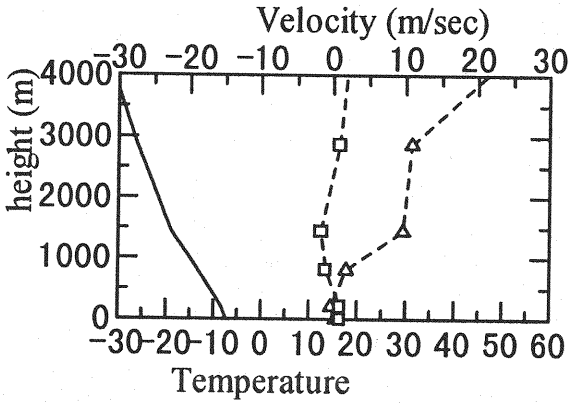

Fig. 16 Radiosonde data at 21:00 on Feb. 17, 1996

The change from a band cloud to low pressure over Ishikari Bay area

The cumulus convection model in this paper is derived using a continuity equation of energy that includes the ratio of non-adiabatic heat. According to Ohyama (9), the ratio of non-adiabatic heat is given using the release energy of a cumulus convection and the ratio depends on the amount of vapor that is converged under the boundary layer:

$$\frac{1}{C_P}Q_1 = \frac{\rho L(C-E)}{C_P} = \rho\pi\eta S w^* \qquad (55)$$

where η = the vertical profile of the amount of latent heat released; and S = vertical decline of the potential temperature. The ratio of non-adiabatic heat (Eq. 55) can easily reproduce a cumulus convection. However it is necessary to the release amount of latent heat. In this model, η (Eq. 56) is derived considering Eq. 53 and Eq. 55. η is obtained by substituting the value of σ_c under a boundary condition into Eq. 56 and considering the state of air.

$$\eta(z) = \frac{a}{\partial\theta_a/\partial z}\sigma_C^2\left(\frac{1}{a}\frac{\partial\theta_a}{\partial z} + \frac{b}{a}\left(\theta_a + \theta_K\right) + 1\right)\left\{1 + \frac{1}{\partial\theta_a/\partial z}\left[a + b\left(\theta_a + \theta_K\right)\right]\right\} \qquad (56)$$

It is the possibility to predict the change from a cumulus convection to a large-scale disturbance such as a typhoon, in regard of whether or not $\eta > 1$. This is called as conditional instability of the second kind(CISK), which is the condition that

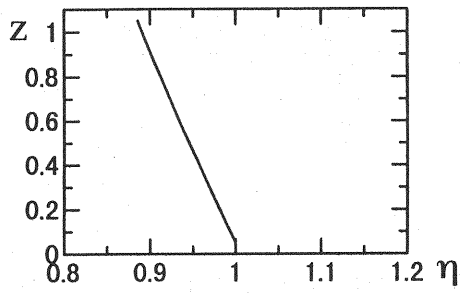

Fig. 17 η at 21:00 on Jan. 7, 1996

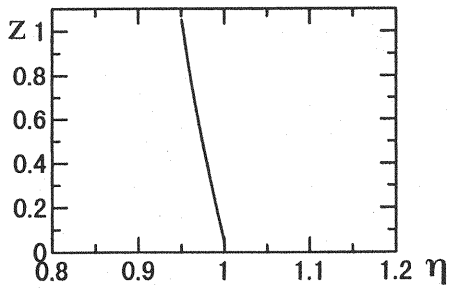

Fig. 18 η at 21:00 on Feb. 17, 1996

determines whether mutual compensation between a cumulus convection and a large-scale disturbance can make a large-scale disturbance into an unstable state.

Snow clouds accompanying a cold air flow may change to low pressure over the Ishikari Bay area. Therefore, this change is estimated by calculating η. Fig. 15 and Fig. 16 show the vertical temperature profile and the vertical wind profile at 21:00 on Jan. 7, 1996 and at 21:00 on Feb. 17, 1996, respectively. On Jan. 7, 1996 low pressure over Ishikari Bay appeared and on Feb. 17, 1996 snow clouds accompanying a cold air flow occurred. Fig. 17 and Fig. 18 show the values of η corresponding to Fig. 15 and Fig. 16, respectively. They indicate that $\eta < 1$, but on Jan. 7, 1996 low pressure over Ishikari Bay occurred and this result does not agree with the actual phenomena. We assume that σ_c can be determined under the condition in which w_c is constant over time. Therefore, we must investigate many cases in which Ishikari low pressure occurs due to changes in w_c.

CONCLUSIONS

(1) Horizontal convection caused by the temperature difference between a cold air flow and the sea is analyzed numerically using the perturbation method. In order for potential flow to be affected by the eddy, which is caused by horizontal convection, the eddy viscosity must be about 1000 m^2/sec. As an eddy viscosity of over 1000 m^2/sec rarely occurs in actual phenomena, the horizontal convection is considered to have no effect on the wind field.

(2) The vertical wind velocity is derived using an entrain and a detrain in a cumulus convection.

(3) A method for predicting the change from a cumulus convection to low pressure over the Ishikari Bay area is proposed considering CISK.

ACKNOWLEDGMENTS

The authors would like to thank the Ishikari Public Sanitation Institute for providing facilities to perform observations. This work was supported by a Grant-in-Aid for the Foundation of River and Watershed Environment Management (K. Nakayama, 8-1-1-1) and a Grant-in-Aid for Developmental Scientific Research provided by MESC (K. Nakayama, 08750617).

REFFERNCES

1. Asai, T. : Study on the convection around atmosphere, Tokyo-do press, 1992.
2. Berson.F.A. : Some measurements on undercutting cold air, Quart. J. Royal Meteo. Soc., Vol.84, pp.1-16, 1958.
3. BRITTER, R.E. and J.E. SIMPSON : Experiments on the dynamics of a gravity vurrent head,J.Fluid Mech., vol.88, pp.223-240, 1978.
4. Ishihara, M., H. Sakakibara and Z. Yanagisawa : Doppler Radar Analysis of the Structure of Mesoscale Snow Bands Developed between the Winter Monsoon, Journal of the Meteorological Society of Japan, pp.503-519, 1989.
5. Kikuchi, K. : Studies on the prediction of heavy snowfall disasters in the urban areas and its reduction and protection, 1993.
6. Nakakita, E., M. Tanaka, M. Shiiba, S. Ikebuchi and T. Takasao : A method of estimating three-dimensional wind velocity and conversion rate of water vapor using information on echo from three-dimensionally scanning radar, , Annual Journal of Hydraulic Engineering, JSCE, VOL.36, pp.483-488, 1992.
7. Nakayama, K., K. Hasegawa and M. Fujita : A study on the shape of a cold air flow around Ishikari Bay in winter at a vertical plane, Annual Journal of Hydraulic Engineering, JSCE, VOL.39, pp.177-182, 1995.
8. Nakayama, K., K. Hasegawa and M. Fujita : Analysis of cold air flow with snow cloud in Ishikari Bay, Journal of Hydraulic, Coastal and Environmental Engineering, No.545, pp.31-42, 1996.
9. Ooyama, K. : A dynamical model for the study of tropical cyclone development, Geof. Inter., pp.187-198, 1961.
10. Ono, F., T. Sugawara, M. Sasamoto, S. Sakai and K. Hirayama : Prediction of snowfall distribution considering effect of wind, Annual Journal of Hydraulic Engineering, JSCE, VOL.34, pp.103-108, 1990.
11. SIMPSON, J.E. : A comparison between laboratory and atmospheric density currents, Quart. J. Royal Meteo. Soc., Vol.95, pp.758-765, 1969.
12. SIMPSON, J.E. and R.E. BRITTER : The dynamics of the head of a gravity vurrent advancing over a horizontal surface, J.Fluid Mech., vol.94, pp.477-495, 1979.
13. TACH IBANA, Y. : Snowfalls and their relation to cold air grainage in Hokkaido Island, Institute of Low Temperature Science, Hokkaido University, January,11,1994.
14. Tsuboki, K., Y. Fujiyoshi and G. Wakahama : Structure of a Land Breeze and Snowfall Enhancement at the Leading Edge, Journal of the Meteorological Society of Japan, pp.757-769, 1989.
15. Tsuboki, K., Y. Fujiyoshi and G. Wakahama : Doppler Radar Observation of Convergence Band Cloud Formed on the West Coast of Hokkaido Island. ‡U:Cold Frontal Type, Journal of the Meteorological Society of Japan, pp.985-999, 1989.

APPENDIX - NOTATION

The following symbols are used in this paper:

ψ = dimensionless stream function;
ω = vorticity;
T = temperature;
a = cubical expansion coefficient of the air;
ν = viscosity coefficient;
κ = thermal diffusivity;
Γ = temperature lapse rate;
x, z = dimensionless horizontal and vertical axis respectively;
h_0 = cold air flow height on coastal line;
U = upper wind velocity;
L = distance of an extended cold air flow;
T_0 = temperature difference between a cold air flow and sea;
Pr = Prandtl number;
ε = the reciprocal of Reynolds number;
α = coefficient of Heaviside function;
a_1, b = coefficient of the approximation of green function;
l = coefficient of the thermal transmission obtained by Bulk coefficient;
(= $C_f U/(2\kappa)\ h_0/T_0$)
C_f = Bulk coefficient;
z_0 = center of vorticity on z-direction;
R, x_0 = front edge of an extended cold air flow on x-direction;
ξ = $x/\varepsilon^{1/2}$; $\eta = z/\varepsilon^{1/2}$;
t = dimensionless time;
$a_0 - a_8$ = coefficient of the approximation of green function;
T = temperature;
q = specific humidity;
h_d = Energy of the dry air;
(= $C_P T + g z$)
h_s = Energy of the moist air;
(= $C_P T + g z + l q$)
$_{c,\ e}$ = a cumulus convection area and a compensation area respectively;
σ_c = ratio of a convection area to all area;
w^* = velocity of z-direction;
t^* = potential temperature;
p = pressure;
g = 9.8 m/sec;
T_{vc^*} = virtual temperature in a convection area;
T_{ve^*} = virtual temperature in a compensation area;
T^* = temperature;
C_P = specific heat;
L = latent heat of condensation;
C = condensation ratio of the vapor;
E = evaporation of the raindrop;

R_d = gas constant;
T_M = temperature difference between the cold air flow and sea;
T_i = 1000 sec; average life time of the snow cloud
h_M = 4000 m; convective cloud height;
w_M = convergence wind;
η = vertical profile of a release amount of latent heat; and
S = vertical decline of the potential temperature.

(Received December 6, 1996; revised January 22, 1998)